Expert Systems with Applications 39 (2012) 7600–7610

Contents lists available at SciVerse ScienceDirect

Expert Systems with Applications

journal homepage: www.elsevier.com/locate/eswa

Vessel segmentation and width estimation in retinal images using multiscale production of matched filter responses

Qin Li [a], Jane You [b,*], David Zhang [b]

[a] Medical Devices and Electronics Testing Center, Shenzhen Academy of Metrology and Quality Inspection, China
[b] Biometrics Research Centre, Department of Computing, The Hong Kong Polytechnic University, KLN, Hong Kong

ARTICLE INFO

Keywords:
Vessel segmentation
Width estimation
Retinal image
Matched filter
Fusion strategy
Multiscale production
Scale selection
Scale normalization

ABSTRACT

Automated segmentation of blood vessels in retinal images can help ophthalmologists screen larger populations for vessel abnormalities. However, automated vessel extraction is difficult due to the fact that the width of retinal vessels can vary from very large to very small, and that the local contrast of vessels is unstable. Further, the small vessels are overwhelmed by Gaussian-like noises. Therefore the accurate segmentation and width estimation of small vessels are very challenging. In this paper, we propose a simple and efficient multiscale vessel extraction scheme by multiplying the responses of matched filters at three scales. Since the vessel structures will have relatively strong responses to the matched filters at different scales but the background noises will not, scale production could further enhance vessels while suppressing noise. After appropriate selection of scale parameters and appropriate normalization of filter responses, the filter responses are then extracted and fused in the scale production domain. The experimental results demonstrate that the proposed method works well for accurately segmenting vessels with good width estimation.

1. Introduction

Images of the ocular fundus, also known as images of the retina, can tell us about retinal, ophthalmic, and even systemic diseases such as diabetes, hypertension, and arteriosclerosis. A critical feature used in such diagnoses is the appearance of blood vessels in ocular fundus (Kanski et al., 2004; Sussman, Tsiaras, & Soper, 1982; Wilkinson et al., 2003). The importance and usefulness of using retinal vessels to help screening Diabetic Retinopathy (DR) have been reported in Staal, Abràmoff, Niemeijer, Viergever, and van Ginneken (2004) and Soares, Leandro, Cesar, Jelinek, and Cree (2006) and the diagnosis of Retinopathy of Prematurity (ROP) by retinal vessel information has been reported in Heneghan, Flynn, O'Keefe, and Cahill (2002) and Gelman, Martinez-Perez, Vanderveen, Moskowitz, and Fulton (2005). The diagnosis of hypertension by automatic grading of retinal vessel tortuosity has been reported in Grisan, Foracchia, and Ruggeri (2008), where the vessel's shape and width are important for diagnosis. The development of an efficient algorithm for automated segmentation of blood vessels in retinal images would help ophthalmologists to screen larger populations for vessel abnormalities. However, automated retinal segmentation is difficult due to the fact that the width of retinal vessels can vary from very large (15 pixels) to very small (3 pixel),[1] and that the local intensity contrast of vessels can be weak and unstable. Further, the small vessels are overwhelmed by Gaussian-like noises. Therefore the accurate segmentation and width estimation of small vessels are very challenging. Many retinal vessel extraction methods have been proposed (Al-Diri, Hunter, & Steel, 2009; Aylward & Bullitt, 2002; Can, Shen, Turner, Tanenbaum, & Roysam, 1999; Chaudhuri, Chatterjee, Katz, Nelson, & Goldbaum, 1989; Frangi et al., 1998; Gelman et al., 2005; Heneghan et al., 2002; Hoover, Kouznetsova, & Goldbaum, 2000; Jiang & Mojon, 2003; Lam & Yan, 2008; Liu & Sun, 1993; Martínez-Pérez, Hughes, & Thom, 2007; Martínez-Pérez et al., 1999; McInerney & Terzopoulos, 2000; Mendonça, Campilho, Centerlines, & Reconstruction, 2006; Perfetti, Ricci, Casali, & Costantini, 2007; Pinz, Bernogger, Datlinger, & Kruger, 1998; Ricci & Perfetti, 2007; Soares et al., 2006; Sofka & Stewart, 2006; Staal et al., 2004; Tamura, Okamoto, & Yanashima, 1988; Toledo et al., 2000; Tolias & Panas, 1998; Vlachos & Dermatas, 2010; Wu, Zhang, Liu, & Bauman, 2006; Zana & Klein, 2001; Zhu, 2010) while it is still very hard to detect the vessels of variant widths simultaneously and the weak, small vessels effectively with good width estimation. This paper will present a simple but efficient multiscale matched filter based scheme to overcome this difficulty.

Vessel segmentation is a specific line detection problem and hence many vessel extraction algorithms are originated from the line detection techniques (Gonzales & Woods, 2007; Lindeberg, 1998; Nikam & Agarwal, 2009; Steger, 1998). Generally speaking, there are two steps in a vessel segmentation scheme. The first step

* Corresponding author. Tel.: +852 2766 7293; fax: +852 2774 0842.
E-mail address: csyjia@comp.polyu.edu.hk (J. You).

[1] We manually cut many vessel cross-sections from the STARE and DRIVE databases to count the vessels' width.

0957-4174/$ - see front matter © 2011 Elsevier Ltd. All rights reserved.
doi:10.1016/j.eswa.2011.12.046

is vessel enhancement and the second step is vessel classification (some methods may go directly to the second step).

In the step of vessel enhancement, the vessels are enhanced and the noises are suppressed. Vessel enhancement is usually implemented locally by using a window centered at the pixel to be enhanced. Actually, this class of techniques is originated from the classical image processing problem: finding edges and ridges in an image (Gonzales & Woods, 2007; Lindeberg, 1998; Nikam & Agarwal, 2009; Steger, 1998). In Chaudhuri et al. (1989), the matched filter was first proposed to detect retinal vessels. The matched filter is an effective technique to enhance vessels by exploiting the prior information that the cross-section of a retinal vessel is Gaussian-shaped. However, the matched filter at a single scale can not effectively enhance all the vessels of variant widths. Even when multiple filters with multiple scales are used, some small and weak vessels still can not be detected due to the low density contrast and relatively heavy background noise. The Gabor filters were also employed to enhance vessels (Soares et al., 2006; Wu et al., 2006). The use of mathematical morphology filters to enhance vessels was reported in Zana and Klein (2001) and Mendonça et al. (2006). The Hessian based methods were reported in Frangi et al. (1998) and Martínez-Pérez et al. (1999, 2007). A Gradient Vector Fields based method was reported in Lam and Yan (2008). In Gelman et al. (2005), the vessels were enhanced through combing morphological filter and the second order derivative operator. In Zhu (2010), the vessel center and borders were found concurrently by analyzing the phase data of the wavelet transforms.

After vessel enhancement, the pixels are classified to vessel pixels and non-vessel pixels. The easiest way is to find an appropriate threshold to classify the pixels according to their intensities. The classification result can be improved at a price of more computation. A threshold probing of the matched filter was proposed in Hoover et al. (2000) to improve the accuracy by analyzing the region-based attributes of the vessel network structure. In Jiang and Mojon (2003), a multi-threshold probing algorithm was applied directly to the original retinal images for classification. The snakes, active contour model and tracking based methods, which utilize not only the intensity information but also the geometrical and topological information, were reported by many researchers to achieve better segmentation with the cost of high computation (Al-Diri et al., 2009; Aylward & Bullitt, 2002; Martínez-Pérez et al., 1999, 2007; Tamura et al., 1988; Vlachos & Dermatas, 2010). In Tolias and Panas (1998), a vessel tracking algorithm based on fuzzy clustering was proposed. In Can et al. (1999), the vessels were segmented through tracking parallel edges. In Aylward and Bullitt (2002), an intensity ridge traversal based method was proposed with the optimization of some major elements in ridge tracking (initialization, noise, singularities, and scale). A region growing scheme was proposed in Martínez-Pérez et al. (1999) and Martínez-Pérez et al. (2007) with the analysis of both spectral information (gradient and curvature) and spatial information. Some supervised learning methods were also reported (Perfetti et al., 2007; Ricci & Perfetti, 2007; Soares et al., 2006; Sofka & Stewart, 2006; Staal et al., 2004).

Among the above methods, the matched filter (Chaudhuri et al., 1989) provides good performance in vessel enhancement. The matched filter is based on the prior knowledge that the cross-section of a retinal vessel is Gaussian-shaped. Therefore a Gaussian-shaped filter can be used to "match" the vessel. If there exists a vessel and its width matches the scale of the filter, a strong response will appear and then the vessel can be detected. Another advantage of the Gaussian-shaped matched filter is that it can smooth noise. In Chaudhuri et al. (1989) and Hoover et al. (2000) a single scale matched filter was used to detect vessels in the retinal image and the scale of the filter was determined by experience. The matched filter with a single scale, however, cannot produce strong responses to all vessels in the retinal image when the width variance is large. To solve this problem, multiscale filters should be introduced.

Some multiscale schemes have been proposed for vessel detection (Frangi et al., 1998; Martínez-Pérez et al., 2007; Mendonça & Campilho, 2006; Soares et al., 2006). In Frangi et al. (1998), the 2-D Gabor filters are applied to retinal images at different scales in order to account for vessels of different widths. In Mendonça and Campilho (2006), a modified top-hat transform was applied to retinal images using circular structuring elements of different radius to detect vessels of different widths. In most of the state-of-the-art multiscale schemes (Martínez-Pérez et al., 2007; Soares et al., 2006; Sofka & Stewart, 2006), the multiscale filter responses were synthesized by taking maximum responses along all scales after appropriate normalization of filter responses at each scale. Those multiscale schemes synthesize the responses of several scales together as the final map of vessels. However, some small and weak vessels still cannot be detected because they are not successfully enhanced at any of the multiple scales. Further, how to extract accurate vessel width has not been sufficiently discussed in these multiscale schemes.

In this paper, we propose a new multiscale vessel extraction scheme by using Multiscale Production of the Matched Filter (MPMF) responses as the multiscale data fusion strategy. The proposed MPMF vessel extraction scheme includes: multiscale matched filtering, scale multiplication in the image enhancement step and double thresholding (Canny, 1986) in the vessel classification step. Considering that the vessel structures will have relatively strong responses to the matched filters at different scales but the background noises will not, multiplying the responses of matched filters at several scales will further enhance the vessels while suppressing the noise. The vessel pixels can then be detected and fused in the scale production domain. This scale multiplication strategy has four advantages. One is that the vessels of variant widths can be detected concurrently because it can incorporate the multiscale information. Secondly, it can detect the small and weak vessels which can not be detected by other methods because the weak vessels could be better enhanced (while the noise being significantly suppressed) in the scale production domain. Thirdly, with scale production and the appropriate selection of scale parameters, the vessel width can better estimated. One more advantage of the proposed method is that it is much easier to implement and has much lower complexity.

The rest of this paper is organized as follows. Section 2 introduces the matched filter and its problems in vessel enhancement. Section 3 presents the proposed multiscale matched filter scheme by using scale production. Section 4 shows the experimental results and Section 5 concludes the paper.

2. Problems in vessel enhancement

As a special case of line detection, the vessel cross-section can be described using either bar model (Steger, 1998) or Gaussian model (Lindeberg, 1998). As shown in Fig. 1(a), the bar model is defined by Eq. (1) where w is the width of a vessel. As shown in Fig. 1(b), the Gaussian model is defined by Eq. (2) where the σ is standard derivation and the width is estimated by 3σ. In this paper, we prefer to analyze using bar model because: (1) there is no single maximum appear in the center of a wide vessel if small size filter is used; (2) most of vessels have sharp edges

$$v(x) = \begin{cases} -h, & |x| \leqslant w, \\ 0, & |x| > w. \end{cases} \tag{1}$$

$$g_\sigma(x) = -\frac{1}{\sqrt{2\pi}\sigma} e^{-\frac{x^2}{2\sigma^2}}. \tag{2}$$

The matched filter for retinal vessel detection was first proposed in Chaudhuri et al. (1989). The 2D matched filter is defined as a

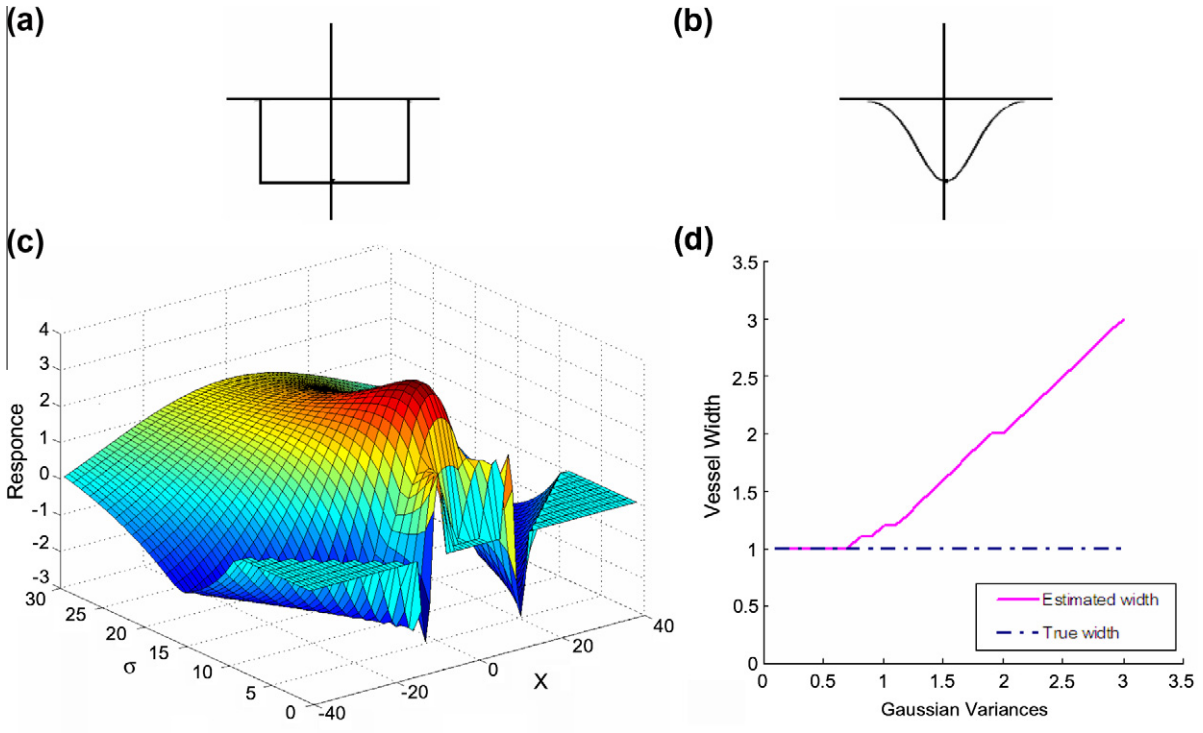

Fig. 1. Multiscale matched filter responses and width estimation.

Gaussian function along the x-axis and this function is repeated in a neighborhood along the y-axis. For easier analysis, we define matched filter using the second derivative of Gaussian similar to Sofka & Stewart (2006). Eq. (3) defines the 1-D matched filter and Eqs. (4) and (5) defines the 2-D matched filter

$$g''_\sigma = \frac{x^2-\sigma^2}{\sqrt{2\pi}\sigma^5} e^{-\frac{x^2}{2\sigma^2}}, \tag{3}$$

$$m_\sigma(x,y) = \frac{x^2-\sigma^2}{\sqrt{2\pi}\sigma^5} e^{-\frac{x^2}{2\sigma^2}}, \quad \text{for } |x| \leqslant 3\sigma, \quad |y| \leqslant L/2, \tag{4}$$

where σ represents the scale of the filter; L is the length of the neighborhood along y-axis to smooth noise. In practice, we will fix L to get square filters and we will rotate $g(x,y)$ to detect the vessels of different orientations and the maximum filter response of all orientations is retained as the final response at that scale. The rotation of $m(x,y)$ with angle ϕ is

$$\begin{cases} m^\phi(x',y') = m(x,y), \\ x' = x\cos\phi + y\sin\phi, \\ y' = y\cos\phi - x\sin\phi. \end{cases} \tag{5}$$

How to select the scale parameter, σ, of the matched filter is a key problem. In Chaudhuri et al. (1989) and Hoover et al. (2000) the scale σ was set as 2 by experience. However, the widths of retinal vessels can vary from very large to very small and using just one scale $\sigma = 2$ can not detect accurately all the vessels. To generate a single maximum response on the center of a line and to achieve good width estimation, the widths of the filter and the line should be constrained in a proper ratio. Following we do the analysis using 1-D model. Matched filter response described using bar model is

$$\begin{aligned} r(x,\sigma,w,h) &= g''_\sigma(x) * v(x) = \int_{-\infty}^{\infty} g''_\sigma(t)\, v(x-t)dt \\ &= \int_{-\infty}^{x-w} g''_\sigma(t)\cdot 0 dt + \int_{x-w}^{x+w} g''_\sigma(t)\cdot(-h)dt + \int_{x+w}^{\infty} g''_\sigma(t)\cdot 0 dt \\ &= h\big(g'_\sigma(x-w) - g'_\sigma(x+w)\big), \end{aligned} \tag{6}$$

where

$$g'_\sigma(x) = \frac{-x}{\sqrt{2\pi}\sigma^3} e^{-\frac{x^2}{2\sigma^2}}. \tag{7}$$

By solving

$$\frac{\partial r(0,\sigma,w,h)}{\partial\sigma} = 0, \tag{8}$$

we have r to exhibit a local maximum at center of a bar if $\sigma \geqslant w/\sqrt{3}$. Fig. 1(c) shows the matched filter responses along scale space (the filter response is normalized and we will discuss normalization later). There is no local maximum at the center of a bar along small scales. Width is estimated as the zero-crossings of the filter response r. The zero-crossings can be found by solving Eq. (9)

$$g'_\sigma(x-w) = g'_\sigma(x+w) \Rightarrow e^{\frac{2xw}{\sigma^2}} = \frac{x+w}{x-w}. \tag{9}$$

This equation can only be solved numerically as illustrated in Fig. 1(d). We can see that the best width is estimated by $\sigma = w/\sqrt{3}$. The larger scale makes the worse width estimation.

In order to segment vessels of variant widths with good noise suppression and good width estimation, an appropriate multiscale scheme is required. The maximum rule is commonly used to fuse multiscale responses (Frangi et al., 1998; Martínez-Pérez et al., 1999, 2007; Soares et al., 2006; Sofka & Stewart, 2006). However, this strategy has two major drawbacks as illustrated in Fig. 2. Fig. 2 simulates the vessel detection by applying multiple matched filters on a retinal image with Gaussian noises. Original signal consists of the cross-sections of several vessels of different width. Noisy signal f is the measurement of the original signal by adding background noise. r_i is the response of the matched filter to f at scale σ_i. As seen in Fig. 1, though both the big and small width vessels can be picked up by taking the maximum responses of all scales, too much noise are preserved and they will deteriorate much the final segmentation result. Further, the width of thin vessel will be over-estimated very much. In following Section 3, we

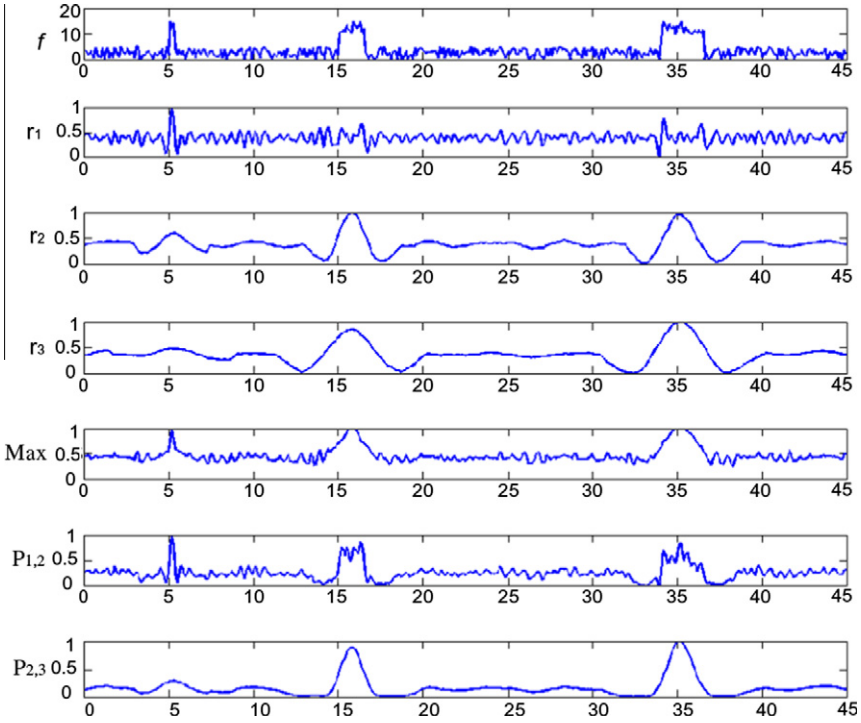

Fig. 2. Multiscale matched filters and scale production. f is the noisy measurement of the original signal; r_1, r_2 and r_3 are the matched filter responses to f at different scales. *Max* means the maximum values among r_1, r_2 and r_3. $P_{1,2}$ is the scale production of r_1 and r_2, and $P_{2,3}$ is the scale production of r_2 and r_3. (Referring to Section 3.1 about P_{12} and P_{23}).

deign a multiscale scheme which is good at noise suppression and width estimation.

3. The multiscale matched filters using scale production

The major problems in vessel enhancement are (1) thin vessels are overwhelmed by Gaussian-like noises; (2) high frequency signal with high energy can pass low frequency band of a "band-pass" filter, such as Gabor filter, or the second derivative of Gaussian, so that a thin vessel's width may be over-estimated. In Mallat and Zhong (1992), Mallat and Zhong illustrated mathematically that signals and noise have different singularities and that edge structures will present observable magnitudes along the scales, while noise will decrease rapidly. This property has been used by Bao et al. in Bao and Zhang (2003) and Bao, Zhang, and Wu (2005) in the applications of noise reduction and edge detection. They used scale production as a strategy to enhance the edges and suppress noise. In this paper, we adopt this idea of scale production of high-pass filters to band-pass filters and propose a multiscale matched filter scheme. The proposed method could be able to detect large and small vessels concurrently. It offers an efficient way to suppress noise so that some small weak vessels with low local contrast can be detected with good width estimation.

3.1. Scale production of the multiscale matched filters

Without loss of generality and for the convenience of expression, we only discuss the multiscale matched filter in the horizontal direction. The filters in other directions can be derived similarly. The response of a matched filter $m_i(x,y)$ to an input image $f(x,y)$ can be expressed by

$$r_i(x,y) = m_i(x,y) * f(x,y). \tag{10}$$

The scale production is defined as the product of filter responses at two different scales

$$P_{i,j}(x,y) = r_i(x,y) \cdot r_j(x,y). \tag{11}$$

Referring to Fig. 2, examples of the scale multiplication of the matched filters are shown. $P_{1,2}$ is the production of the filter responses at scales 1 and 2, while $P_{2,3}$ is the production of the filter responses at scales 2 and 3. We can see that the vessel structures have relatively strong responses to the matched filters at scales 1, 2, and 3. But the background noises were smoothed a lot at scales 2 and 3. So, multiplying the responses of matched filters at different scales will enhance the vessels while suppressing the noise. Consequently, the filter responses to vessels of all widths can be better enhanced in $P_{1,2}$ and $P_{2,3}$ than in r_1, r_2 and r_3. The noise is also better suppressed in $P_{1,2}$ and $P_{2,3}$. The width of thin vessels will be enlarged by large scale filters. Interestingly, this distortion could be corrected to some extent by employing a smaller scale filter in the scale production, as we can see in $P_{1,2}$. Finally, the vessels of variant widths and noise can be more easily discriminated in the scale production than in the original filter responses by using a simple thresholding strategy.

Based on the above observation and discussion, in our multiscale matched filters, the production $P_{1,2}$ is used to extract small, thin vessels and the production $P_{2,3}$ is used to extract big, wide vessels after thresholding. We will then get two binary vessel maps and they are directly fused by using an "OR" logic operation to yield the final vessel map. The key issue in our scheme is the selection of scale parameters. In the following Section 3.2, we will discuss how to select appropriate scale parameters.

3.2. Multiscale selection

Before selection of scales, the filter responses have to be normalized first because the response energies of spatial operators such as Gabor filter or the matched filter generally decrease with increasing scale. With good normalization, the global maximum of multiscale responses of a vessel of particular width will appear

at an appropriate scale so that the vessel can be better enhanced with good width estimation referring to Fig. 1(c) and (d). The normalization using Gaussian model line has been well analyzed in Sofka and Stewart (2006) and Lindeberg (1998) by employing a normalization multiplier σ^{α}. The α was solved to be 3/4 in Sofka and Stewart (2006) and Lindeberg (1998). However, because the vessel cross-section can not be perfectly modeled by a Gaussian, we derive the normalization multiplier using the bar model. Eq. (12) is the center filter response produced by convolving the second derivative of Gaussian whose standard variation is σ with the bar whose width is w

$$r(0,\sigma,w,h) = h(g'_{\sigma}(-w) - g'_{\sigma}(w)). \tag{12}$$

The normalization is defined by Eq. (13). The peak of Eq. (13) can be found by solving Eq. (14).

$$r_{\alpha-norm}(0,\sigma,w,h) = \sigma^{\alpha} r(0,\sigma,w,h), \tag{13}$$

$$\frac{\partial r_{\alpha\text{-}norm}(0,\sigma,w,h)}{\partial\sigma} = 0 \quad \Rightarrow \quad \sigma = \frac{w}{\sqrt{3-\alpha}}. \tag{14}$$

We have $\alpha = 2$ if $\sigma = w$.

In fact, vessel may be regarded as a bar smoothed by a Gaussian, so the normalization should be set as $3/4 < \alpha < 2$. Small α cannot give large scale filter enough compensation but large α will overestimate width. In our experiments, we empirically found that setting α around 5/4 is a good balance between filter peak response and width estimation.

Using normalized filter responses, we can find appropriate scales to enhance vessels of different widths. In our three-scale scheme, ideally, we set scale 1 is the best scale to enhance the thinnest vessel and we set scale 3 is the best scale to enhance the widest vessel. And we set a middle scale which satisfies three criteria: (1) it can denoise for enhance thin vessel; (2) it does not over-estimate thin vessel width much; and (3) it can give reasonable response for both small and wide vessel. Following we describe how to find this middle scale. The center matched filter response described using bar model is defined in Eq. (15)

$$\begin{aligned} r_{\alpha\text{-}norm}(0,\sigma,w,h) &= \sigma^{\alpha}\cdot h(g'_{\sigma}(-w) - g'_{\sigma}(w)) \\ &= \sigma^{\alpha}\cdot h\left(\frac{w}{\sqrt{2\pi}\sigma^3}e^{-\frac{w^2}{2\sigma^2}} - \frac{-w}{\sqrt{2\pi}\sigma^3}e^{-\frac{w^2}{2\sigma^2}}\right) = \frac{2hw\sigma^{\alpha-3}}{\sqrt{2\pi}}e^{-\frac{w^2}{2\sigma^2}}. \end{aligned} \tag{15}$$

Denoting the widths of the thinnest and widest vessels as a and b respectively, the σ of the middle scale can be found by solving Eq. (16) with respecting to the three criteria above

$$a\cdot e^{-\frac{a}{2\sigma^2}} - b\cdot e^{-\frac{b^2}{2\sigma^2}} = 0 \quad \text{and} \quad \sigma \geqslant b/\sqrt{3}. \tag{16}$$

Because the bar-model may not describe vessel perfectly, we find the middle scale by learning the retinal database STARE (Chaudhuri et al., 1989; Hoover et al., 2000) and DRIVE (Staal et al., 2004). We manually cut 100 cross-sections of the thinnest/widest vessels and use the averaging as model to describe thinnest/widest vessel. And then we use the learned vessel model to produce filter response $r_{\alpha\text{-}norm}(0,\sigma,a,1)$ and $r_{\alpha\text{-}norm}(0,\sigma,b,1)$. Finally the middle scale can be numerically solved by finding the cross of $r_{\alpha\text{-}norm}(0,-\sigma,a,1)$ and $r_{\alpha\text{-}norm}(0,\sigma,b,1)$. This procedure is illustrated in Fig. 3. Please note that the width of thinnest/widest vessels can be roughly regarded as 1 and 7 in STARE and DRIVE databases. That makes Eq. (16) is solvable.

Fig. 4 shows an example of the proposed scale production with comparison to the maximum rule. It is seen that scale production can better discriminate vessels from background noise while the max rule can introduce many false vessel pixels.

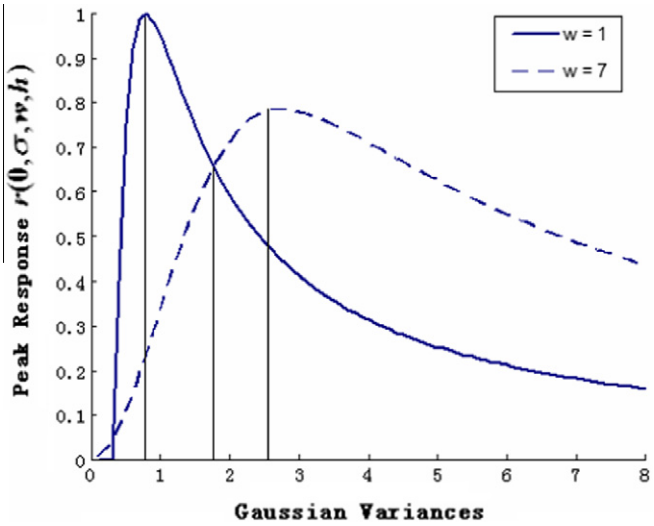

Fig. 3. Filter peak responses to the thinnest and widest vessels along scale space.

3.3. Thresholding

After determining the three matched filters of variant scales, we apply them to the retinal image and obtain three responses. The responses are multiplied and two scale production images are obtained. As illustrated in Figs. 2 and 4 the responses to vessel structures are enlarged while the responses to noise are weakened. A simple single-thresholding or double-thresholding (Canny, 1986) operation could effectively distinguish vessels from noise. Because double-thresholding can better suppress noise with preserving the connectivity of lines and edges, in this paper we adopt this strategy and apply it to both $P_{1,2}$ and $P_{2,3}$. Take $P_{1,2}$ for example, with double-thresholding a low threshold t_l and a high threshold $t_h = 2t_l$ are imposed on $P_{1,2}$ and then two vessels maps V_l and V_h are obtained. The vessel map of $P_{1,2}$ will be formed by selecting vessels in V_l that link to the vessels in V_h. The same procedure goes to $P_{2,3}$ and the final vessel map is made by fusing the outputs of $P_{1,2}$ and $P_{2,3}$ with "OR" logic operation.

3.4. Post-processing

After double-thresholding, some post-processing operations are used to improve the segmentation accuracy. Fig. 5(b) shows a retinal image segmented by the proposed MPMF scheme. We can see that there are some false positives caused by bright lesions and some unlinked small vessels. In this section, we implement some simple post-processing procedures to solve those problems to some extent.

3.4.1. Eliminating the false positives caused by bright lesions

Because the matched filter responses not only to Gaussian-shaped lines but also to step edges, the bright lesions can cause false positives. In Can et al. (1999), the vessels were extracted by tracing parallel edges. In their model, for each vessel pixel, there should be two edge pixels along the normal direction, and the gradient direction of the two edge pixels should be opposite to each other (both of them should point outward normal). We adopt this parallel-edge vessel model in the post-processing of the proposed MPMF scheme. For each vessel pixel classified by the MPMF, i.e. for each white pixel in Fig. 5(b), we find the pair of boundary pixels along the normal direction of the vessel. The normal direction is defined as the direction with maximum matched filter response. The boundary pixels are simply generated by subtracting

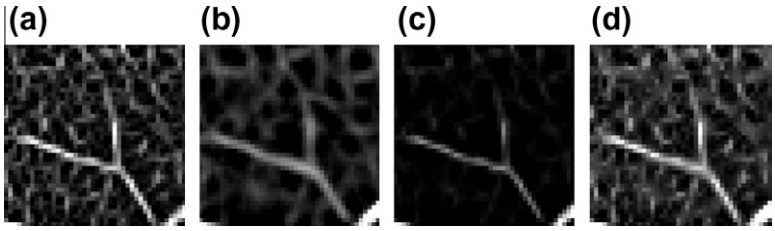

Fig. 4. (a) and (b) matched filter responses at different scales; (c) is the scale production of (a) and (b); (d) is the maximum of filter responses along scales.

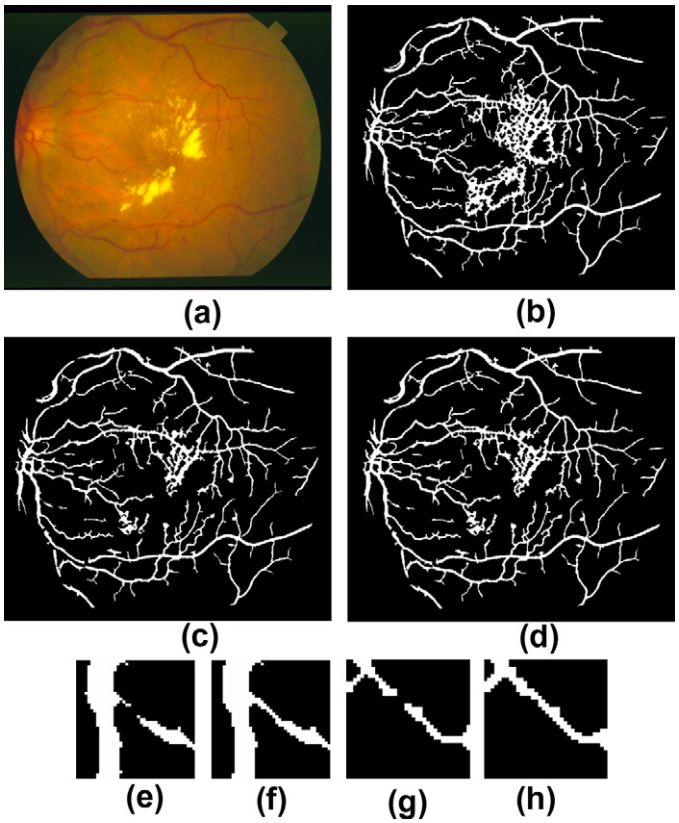

Fig. 5. The vessel segmentation and postprocessing of a retinal image with bright lesion by MPMF. (a) The original image in STARE database (Chaudhuri et al., 1989; Hoover et al., 2000); (b) vessel segmentation result by MPMF; (c) suppress false positives caused by bright lesions; (d) link small broken vessels; (e) and (g) are cropped and enlarged images from (c); (f) and (h) are cropped and enlarged images from (d).

Fig. 5(b) from its dilated version. The gradient map is generated using canny operator. If the gradient direction of both the two boundary pixels is pointing outward normal, the current vessel pixel is classified as a true positive. Otherwise it is classified as a false positive. Fig. 5(c) shows the false positive eliminating result of Fig. 5(b).

3.4.2. Linking broken vessels

The broken vessels in Fig. 5(b) are caused by the vessels with discontinuous intensities, especially, the small vessels whose intensities are very close to background. Though the matched filter has already smoothed the intensity along tangent direction of vessels, some pixels' responses are still too weak to distinguish them from noise. Here we use an anisotropic morphological operation to link the broken vessels segmented by MPMF. First, we segment the scale production using a very low threshold $t_{vl} = \alpha t_l$, where α is a constant (we set $\alpha = 0.3$ in this paper). The pixels within interval

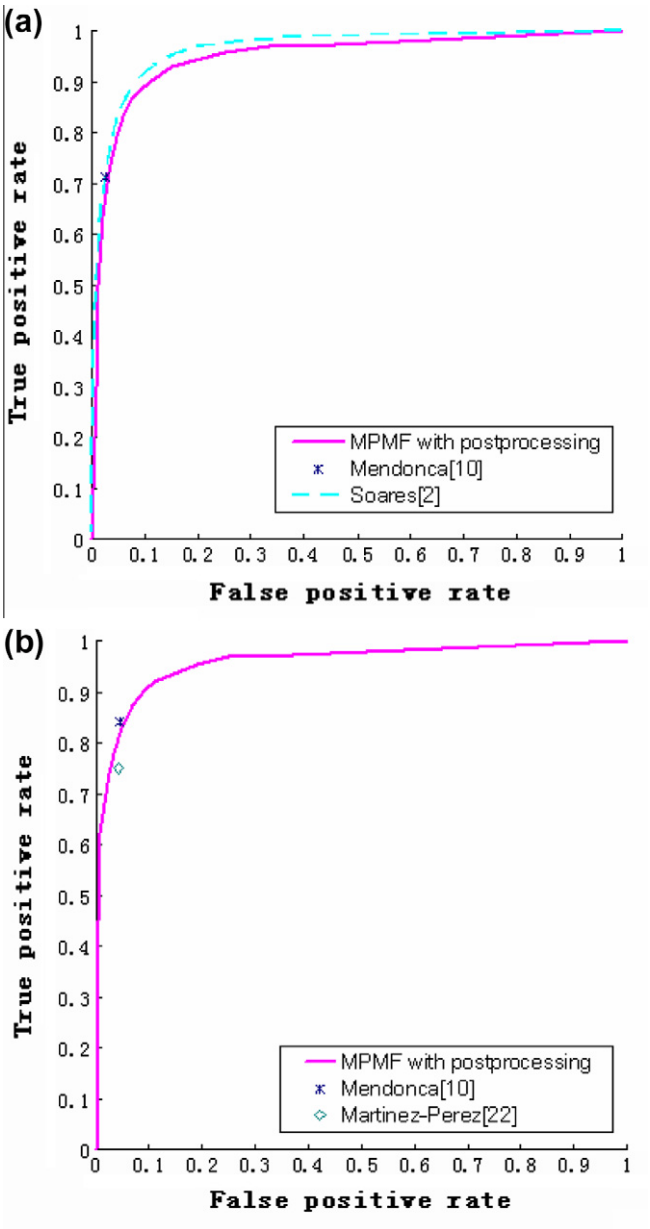

Fig. 6. System evaluation using ROC curve for STARE database. (a) Computed with FOV; and (b) computed without FOV.

$[t_{vl}, t_l]$ are defined as potential vessel pixels to be linked. At each potential vessel pixel, we apply morphological closing using linear structure. The direction of the linear structure is perpendicular to the direction of maximum matched filter response. We set the length of the linear structure as 9 pixels in the experiments. Fig. 5(d) shows the vessel linking result of Fig. 5(c). For a better

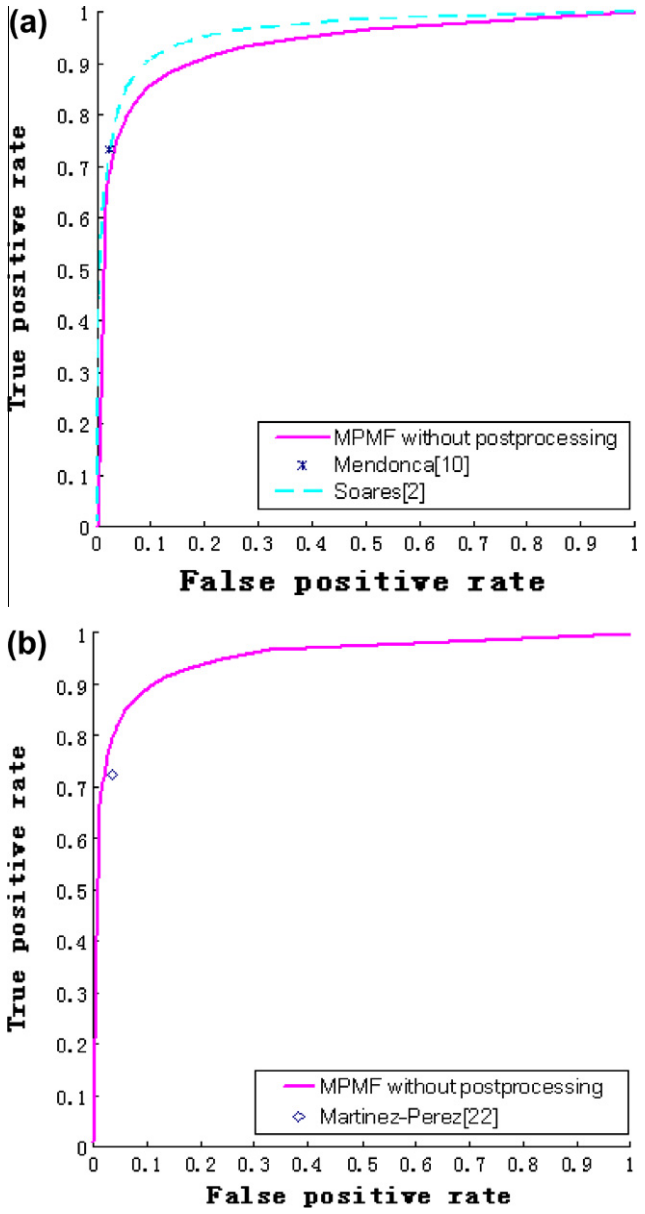

Fig. 7. System evaluation using ROC curve for DRIVE database (Staal et al., 2004). (a) Computed with FOV; and (b) computed without FOV.

Table 1
Extraction results for 20 images in STARE Database (with FOV).

Method	Accuracy	TPR	FPR
Second human observer	0.9354	0.8949	0.0610
Hoover et al. (2000)	0.9267	0.6751	0.0433
Staal et al. (2004)	0.9516	0.6970	0.0190
Soares et al. (2006)	0.9480	0.7165	0.0252
Mendonça and Campilho (2006)	0.9479	0.7123	0.0242
MPMF with postprocessing	**0.9407**	**0.7191**	**0.0313**

visual perception, we crop and zoom-in part of the images in Fig. 5(c) and (d) and show them in Fig. 5(e)–(h).

4. Experimental results

We test the proposed automated vessel segmentation method using the open STARE and DRIVE databases (Chaudhuri et al., 1989; Hoover et al., 2000; Staal et al., 2004). The STARE database consists of retinal images captured by the TopCon TRV-50 fundus camera at 35° FOV, which were digitized at 24-bits with a spatial resolution of 700×605 pixels. There are 20 images for vessel detection. Ten of them are from healthy ocular fundus and the other 10 are from unhealthy ones. The database also provides hand-labeled images as the ground truth for vessel segmentation so that the algorithms can be evaluated for comparison. The DRIVE databases consists of 40 images captured by the Canon CR5 camera at 45° FOV, which were digitized at 24-bits with a spatial resolution of 565×584 pixels. Seven images are abnormal. Hand-labeled images are also available in this database.

Figs. 6 and 7 compare the proposed MPMF with other methods employing multiscale filters: multiscale Gabor filters with supervised classification proposed by Soares et al. (2006), multiscale morphological filters with centerline detection proposed by Mendonça and Campilho (2006), and the multiscale Hessian with region growing proposed by Martínez-Pérez et al. (2007).[2] The

Table 2
Extraction results for 20 images in STARE Database (without FOV).

Method	Accuracy	TPR	FPR
Second human observer	0.9522	0.8947	0.0438
Hoover et al. (2000)	N.A.	0.7500	0.0438
Mendonça and Campilho (2006)	N.A.	0.8420	0.0438
Martínez-Pérez et al. (2007)	0.9410	0.7506	0.0431
MPMF with postprocessing	**0.9461**	**0.8069**	**0.0422**

Table 3
Extraction results for 20 images (test set) in DRIVE Database (with FOV).

Method	Accuracy	TPR	FPR
Second human observer	0.9473	0.7761	0.0275
Staal et al. (2004)	0.9442	0.7194	0.0227
Soares et al. (2006)	0.9466	0.7283	0.0212
Martínez-Pérez et al. (2007)	0.9463	0.7315	0.0219
MPMF without postprocessing	**0.9343**	**0.7154**	**0.0284**

Table 4
Extraction results for 20 images (test set) in DRIVE Database (without FOV).

Method	Accuracy	TPR	FPR
Second human observer	0.9637	0.7757	0.0181
Martínez-Pérez et al. (2007)	0.9344	0.7246	0.0345
MPMF without postprocessing	**0.9496**	**0.7843**	**0.0324**

Table 5
Extraction results for 20 images in STARE Database (with FOV) (normal versus abnormal cases).

Method	Accuracy	TPR	FPR
Normal cases			
Second human observer	0.9283	0.9646	0.0764
Hoover et al. (2000)	0.9324	0.6766	0.0338
Mendonça and Campilho (2006)	0.9531	0.7366	0.0178
MPMF with postprocessing	**0.9504**	**0.7929**	**0.0279**
Abnormal cases			
Second human observer	0.9425	0.8252	0.0456
Hoover et al. (2000)	0.9211	0.6736	0.0528
Mendonça and Campilho (2006)	0.9426	0.6801	0.0306
MPMF with postprocessing	**0.9310**	**0.6455**	**0.0337**

[2] The results of Mendonça et al. (2006) and Martínez-Pérez et al. (2007) are obtained from their original papers. The results of Soares et al. (2006) are from the author' help.

Table 6
Running time per image in STARE database.

Method	System environment	Running time
Soares et al. (2006)	P-III 1.5GHz, 512 Mb RAM, Matlab	3.5 min
Mendonça and Campilho (2006)	P-IV 3.2GHz, 960 Mb RAM, Matlab	3 min
MPMF without postprocessing	P-III 1.5GHz, 512 Mb RAM, Matlab	8 s
MPMF with postprocessing	P-III 1.5GHz, 512 Mb RAM, Matlab	0.5 min

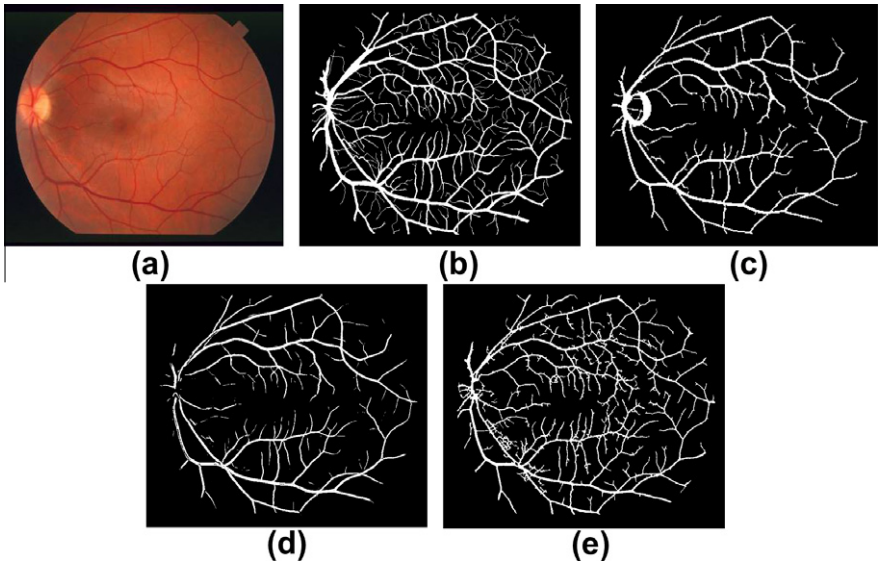

Fig. 8. (a) The original image im0255 in the STARE database; (b) the ground truth vessel map; the extraction results by (c) Martínez-Pérez et al. (2007), Accuracy = 0.8957, Sensitivity = 0.4780, Predictive = 0.9278; (d) Soares et al. (2006), Accuracy = 0.9117, Sensitivity = 0.5144, Predictive = 0.9461; and (e) the proposed MPMF, Accuracy = 0.9204, Sensitivity = 0.7169, Predictive = 0.9060.

ROC curves are obtained by plotting true positive rate (TPR) against false positive rate (FPR). In Figs. 6(a) and 7(a), the TPR is defined as the ratio of the number of correctly classified vessel pixels to the number of total vessel pixels in the ground truth. The FPR is defined as the ratio of the number of non-vessel pixels inside FOV but classified as vessel pixels to the number of non-vessel pixels inside FOV in the ground truth. To compare with Martínez-Pérez et al. (2007), in Figs. 6(b) and 7(b), we replicated the computation conditions by considering all image pixels (without FOV).

Fig. 6 shows the results for STARE database (Chaudhuri et al., 1989; Hoover et al., 2000). We can see that our method is better than Martínez-Pérez et al. (2007) and is comparable to Soares et al. (2006) and Mendonça and Campilho (2006).

Fig. 7 shows the results for DRIVE database (Staal et al., 2004). In order to show the benefits from scale production, our ROC curve is generated by using MPMF without any postprocessing described in Section 3.4. We can see that MPMF without any postprocessing is better than Martínez-Pérez et al. (2007) and is comparable to Soares et al. (2006) and Mendonça and Campilho (2006). That means the simple scale production can improve the signal-to-noise ratio a lot.

Tables 1–5 compare the proposed MPMF method with the state-of-the-art schemes (Hoover et al., 2000; Martínez-Pérez et al., 2007; Mendonça and Campilho, 2006; Soares et al., 2006; Staal et al., 2004) by using the performance measures (1) detection accuracy, and the corresponding (2) true positive rate (TPR) and (3) false positive rate (FPR) at that accuracy.[3] In Tables 1, 3 and 5, the detection accuracy is defined as the ratio of the total number of correctly classified pixels (the vessel pixels classified as vessel pixels and the non-vessel pixels classified as non-vessel pixels) to the number of pixels inside FOV. The TPR is defined as the ratio of the number of correctly classified vessel pixels to the number of total vessel pixels in the ground truth. The FPR is defined as the ratio of the number of non-vessel pixels inside FOV but classified as vessel pixels to the number of non-vessel pixels inside FOV in the ground truth. To compare with Martínez-Pérez et al. (2007), in Tables 2 and 4, we replicated the computation conditions by considering all image pixels (without any FOV).

Table 1 presents the performance of MPMF on STARE database (Chaudhuri et al., 1989; Hoover et al., 2000). The results of Staal et al. (2004), Mendonça and Campilho (2006) and Martínez-Pérez et al. (2007) are obtained from their papers. The performance measures of Soares et al. (2006) and Hoover et al. (2000) are calculated using the segmented images obtained from their websites. The FOV used for STARE database is generated using the code provided by Soares et al. (2006).[4] All 20 images are used in the experiment. The hand-labeled images by the first human expert (labels-ah) are used as ground truth.

[3] Parts of the results of those methods are obtained from the original papers. For some methods, only the result on STARE or DRIVE database was available.

[4] We thank Dr. Soares for sharing his codes.

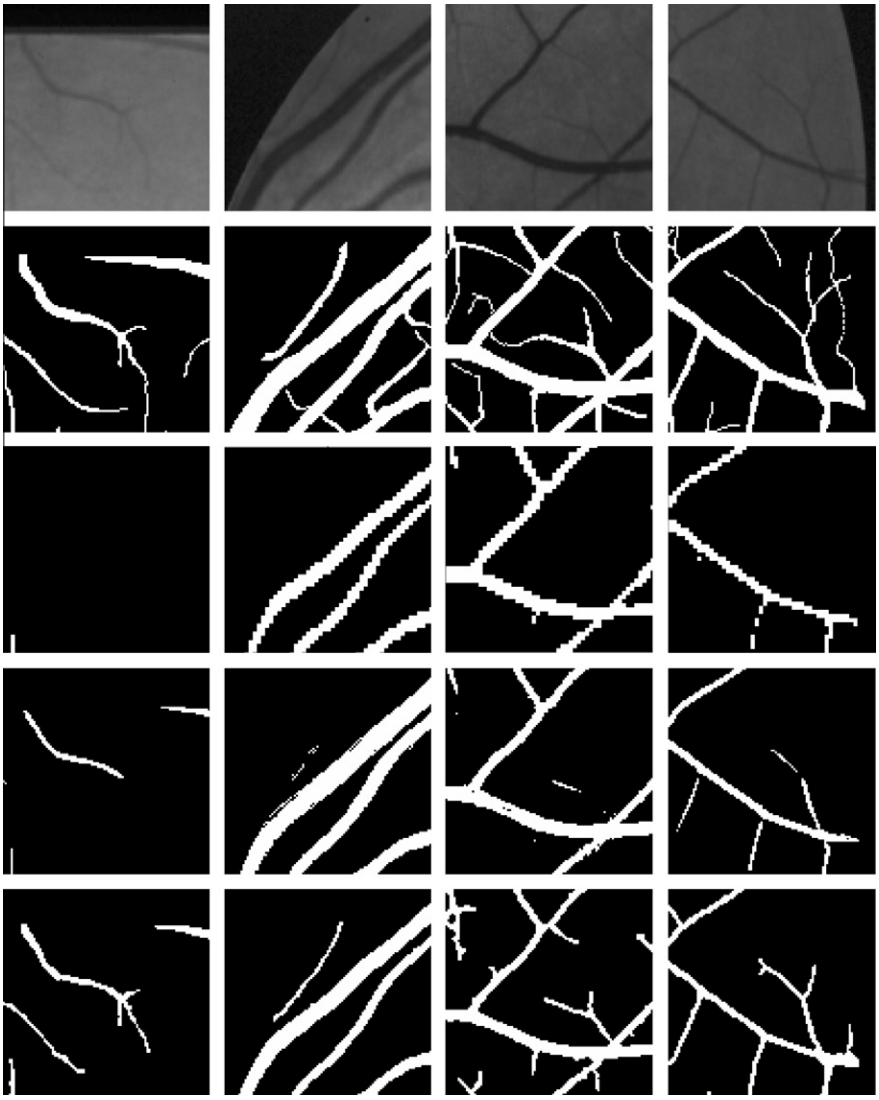

Fig. 9. Zoom-in subimages in the STARE database. The first row shows some cropped blocks from the original images; the second row shows their corresponding ground truth vessel maps; the third row shows the vessel extraction results using method by Martínez-Pérez et al. (2007); the fourth row shows the results using method by Soares et al. (2006); and the fifth row shows the results using the proposed MPMF method.

Table 2 presents the performance of MPMF on STARE database (Chaudhuri et al., 1989; Hoover et al., 2000) without considering FOV. To facilitate the comparison of our method with those proposed by Hoover et al. (2000), Mendonça and Campilho (2006) and Martínez-Pérez et al. (2007), we calculated the average true positive rate corresponding to a false positive rate around 0.04.

Table 3 presents the performance of MPMF on DRIVE database (Staal et al., 2004). In order to show the benefits from scale production, our results are generated by using MPMF without any postprocessing described in Section 3.4. The results of Staal et al. (2004) and Soares et al. (2006) are calculated using the segmented images obtained from their websites. The results of Mendonça and Campilho (2006) and Martínez-Pérez et al. (2007) are obtained from their papers. The DRIVE database provides FOV. All 20 images in the test set are used in the experiment. The hand-labeled images by the first human expert (2nd_manual) are used as ground truth.

Table 4 presents the performance of MPMF on DRIVE database (Staal et al., 2004) without considering FOV. To facilitate the comparison of our method with the method proposed by Martínez-Pérez et al. (2007), we calculated the average true positive rate corresponding to a false positive rate around 0.03.

Table 5 presents the different performances of the proposed MPMF for normal and abnormal images in STARE database (Chaudhuri et al., 1989; Hoover et al., 2000). The results of Soares et al. (2006) and Hoover et al. (2000) are calculated using the segmented images obtained from their websites. The result of Mendonça and Campilho (2006) is obtained from the original paper.

From Tables 1–5, we can see that the proposed MPMF method is competitive with those state-of-the-art methods. The MPMF without any postprocessing achieves better results than the multiscale method proposed by Martínez-Pérez et al. (2007). That shows the scale production is a good strategy to fuse multiscale "band-pass" filter responses. It should be noted that the proposed MPMF method is much easier to implement and has much lower complexity. A real-time system can benefit from our method. Table 6 shows the running time of our method with comparison to some recent published works (Mendonça and Campilho, 2006; Soares et al., 2006).[5]

Since the large vessels are relatively easier to be detected and

[5] To compare with Soares et al. (2006), we download the authors' code and tested on our machine; to compare with Mendonça et al. (2006), we use the data in that paper.

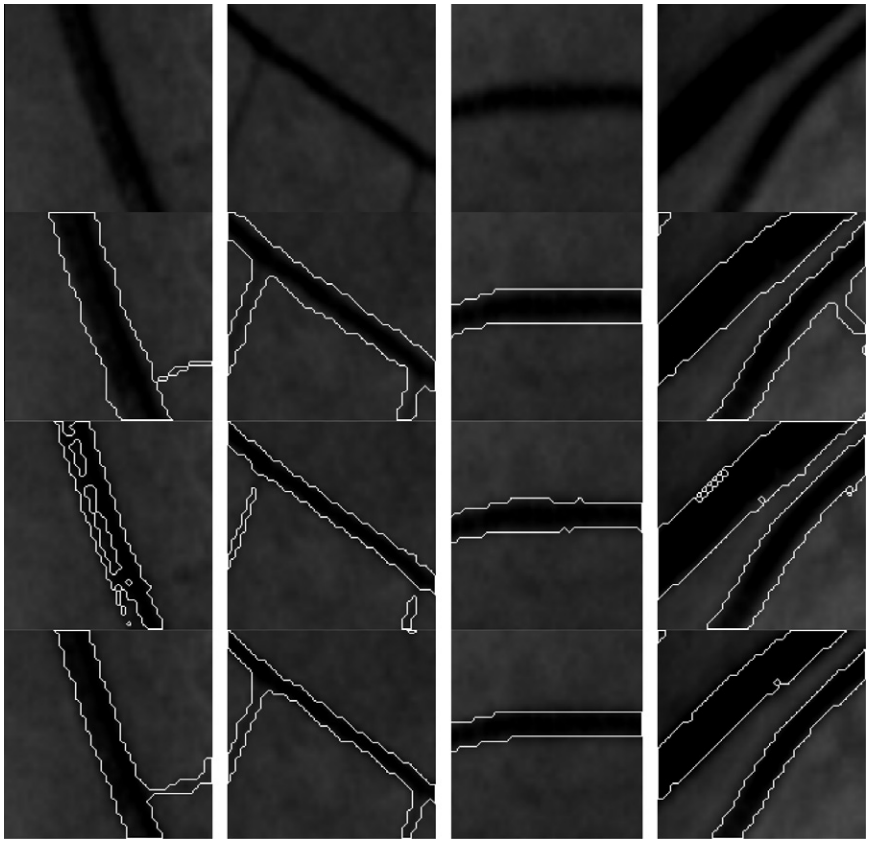

Fig. 10. The first row shows some zoomed and enhanced blocks from the original images in STARE database; the second, third, and fourth rows show the respective borders of segmentations by the second observer (Hoover et al., 2000; Soares et al., 2006), and MPMF.

they occupied most of the white pixels in the ground truth, the performances of different methods can not be well evaluated by the quantitative results described using Accuracy, TPR, and FPR. Figs. 8–10 give some visual inspections to evaluate the performance of our method in improving signal-to-noise ratio and width estimation. Fig. 8 shows the vessel segmentation results on the image *im0255* in the STARE database (Chaudhuri et al., 1989; Hoover et al., 2000) using the four schemes: the multiscale Gabor filters with supervised classification proposed by Soares et al. (2006), the multiscale Hessian with region growing proposed by Martínez-Pérez et al. (2007), the multiscale matched filter with max rule and the proposed MPMF. The segmented results of Soares et al. (2006) and Martínez-Pérez et al. (2007) were obtained from their websites. Because results of Martínez-Pérez et al. (2007) were down-sampled on the website, we resized the images for comparison. That causes some artifacts around the edges of vessels. But that will not affect the general view of the vessel map very much. We vary the threshold to achieve sensitivity as high as possible at the smallest cost of accuracy. The proposed MPMF achieves the highest sensitivity at the accuracy similar to other schemes. It is seen that the methods proposed by Soares et al. (2006) and Martínez-Pérez et al. (2007) miss many thin vessels; the multiscale scheme with the max rule extracts some thin vessels but also introduces some false vessels due to noise; the proposed MPMF scheme can find many weak and thin vessels which can not be found by the other three schemes.

For a better visual evaluation of the proposed scheme, we crop several parts of the images in the STARE database and zoom-in them in Fig. 9. The first row shows the original cropped images; the second row shows their corresponding ground truth vessel maps; the third row shows the vessel extraction results by Martínez-Pérez et al. (2007); the fourth row shows the results using Soares' supervised method (Soares et al., 2006); the fifth row shows the results by using the Max rule over three scales; the bottom row shows the results of MPMF. We see that MPMF scheme can extract both thin and wide vessels simultaneously. The low contrast weak vessel can also be extracted from the noisy background using MPMF.

Fig. 10 evaluates width estimation by superimpose the detected vessel borders on the original images. The first row of Fig. 10 shows some zoomed blocks from the original images in STARE database (Chaudhuri et al., 1989; Hoover et al., 2000) the second, third, and fourth rows superimpose the respective vessel borders detected by the second observer Hoover et al. (2000) and Soares et al. (2006), and MPMF on the original images. From Fig. 10, we can see that the vessel borders found by the second observer, i. e. the ground truth (Hoover et al., 2000), frequently over-estimate the vessel widths. Comparing to that, the borders found by MPMF appear to match better the real vessel borders.

5. Conclusion and further work

We proposed a multiscale retinal vessel extraction scheme MPMF by multiplying the responses of matched filters at three scales. Since the vessels will have relatively strong responses to the matched filters along scale space while the background noises decreasing rapidly, scale production could enhance vessels while suppressing noise. Further, with appropriate selection of scale parameters in MPMF, our method achieves good width estimation. We have also derived an appropriate theoretical range to facilitate the normalization of retinal vessels' filter responses. We demon-

strated that scale production is an efficient strategy to fuse multi-scale "band-pass" filter responses by picking up vessel pixels in the scale production domain and then proposed a simple but effective retinal vessel detection scheme. The experimental results validate that the proposed MPMF method can extract both wide and thin vessels concurrently and can extract low contrast weak vessels, which can not be detected by other schemes, with low computational complexity. The low computational complexity makes real-time applications possible. And the good width estimation is helpful in diagnosis of retinal tortuosity.

However, there is a chance that the middle scale can not be found for particular databases. In that case, we have to make a larger in Eq. (16) of Section 3.2. That will result in lost of thin vessels. We believe that only three scales are not enough to segment accurately all vessels. In the future, we will modify MPMF to have more scales for better vessel enhancement. Another problem of MPMF is the false positives caused by lesions in a retina. We will try adapting MPMF to the tracking based methods, such as (Aylward & Bullitt, 2002; Tamura et al., 1988), or the supervised methods, such as (Soares et al., 2006; Sofka & Stewart, 2006; Staal et al., 2004). By removing the lesions and improving the connectivity of vessels, the vessels of variant widths could be more accurately detected.

Acknowledgement

The authors are most grateful for the constructive advice on the revision of the manuscript from the anonymous reviewers. The funding supports from Hong Kong Government under its GRF scheme (5341/08E and 5366/09E) are greatly appreciated. And the research grant from Hong Kong Polytechnic University (1-ZV5U and G-U883) and Shenzhen Academy of Metrology and Quality Inspection are also greatly appreciated.

References

Al-Diri, B., Hunter, A., & Steel, D. (2009). An active contour model for segmenting and measuring retinal vessels. *IEEE Transactions on Medical Imaging, 28*, 1488–1497.

Aylward, S. R., & Bullitt, E. (2002). Initialization, noise, singularities, and scale in height ridge traversal for tubular object centerline extraction. *IEEE Transactions on Medical Imaging, 21*(2), 61–75.

Bao, P., & Zhang, L. (2003). Noise reduction for magnetic resonance image via adaptive multiscale products thresholding. *IEEE Transactions on Medical Imaging, 22*, 1089–1099.

Bao, P., Zhang, L., & Wu, X. L. (2005). Canny edge detection enhancement by scale multiplication. *IEEE Transactions on Pattern Analysis and Machine Intelligence, 27*(9), 1485–1490.

Can, A., Shen, H., Turner, J. N., Tanenbaum, H. L., & Roysam, B. (1999). Rapid automated tracing and feature extraction from retinal fundus images using direct exploratory algorithms. *IEEE Transactions on Information Technology in Biomedicine, 3*(2), 125–138.

Canny, J. (1986). A computational approach to edge detection. *IEEE Transactions on Pattern Recognition and Machine Intelligence, 8*, 679–698.

Chaudhuri, S., Chatterjee, S., Katz, N., Nelson, M., & Goldbaum, M. (1989). Detection of blood vessels in retinal images using two-dimensional matched filters. *IEEE Transactions on Medical Imaging, 8*, 263–269.

Frangi, A., Niessen, W. J., Vincken, K. L., & Viergever, M. A. (1998). Multiscale vessel enhancement filtering. In *Proceedings of the first MICCAI* (pp. 130–137).

Gelman, R., Martinez-Perez, M. E., Vanderveen, D. K., Moskowitz, A., & Fulton, A. B. (2005). Diagnosis of plus disease in retinopathy of prematurity using retinal image multiscale analysis. *Investigative Ophthalmology and Visual Science, 46*, 4734–4738.

Gonzales, R. C., & Woods, R. E. (2007). *Digital image processing* (3rd ed.). Prentice Hall.

Grisan, E., Foracchia, M., & Ruggeri, A. (2008). A novel method for the automatic grading of retinal vessel tortuosity. *IEEE Transactions on Medical Imaging, 27*, 310–319.

Heneghan, C., Flynn, J., O'Keefe, M., & Cahill, M. (2002). Characterization of changes in blood vessel width and tortuosity in retinopathy of prematurity using image analysis. *Medical Image Analysis, 6*, 407–429.

Hoover, A., Kouznetsova, V., & Goldbaum, M. (2000). Locating blood vessels in retinal images by piecewise threshold probing of a matched filter response. *IEEE Transactions on Medical Imaging, 19*(3), 203–210.

Jiang, X., & Mojon, D. (2003). Adaptive local thresholding by verification based multithreshold probing with application to vessel detection in retinal images. *IEEE Transactions on Pattern Analysis and Machine Intelligence, 25*(1), 131–137.

Kanski, J., Milewski, S., Damato, B., & Tanner, V. (2004). *Diseases of the ocular fundus.* Mosby: Elsevier.

Lam, B., & Yan, H. (2008). A novel vessel segmentation algorithm for pathological retina images based on the divergence of vector fields. *IEEE Transactions on Medical Imaging, 27*, 237–246.

Lindeberg, T. (1998). Feature detection with automatic scale selection. *International Journal of Computer Vision, 30*, 79–116.

Liu, I., & Sun, Y. (1993). Recursive tracking of vascular networks in angiograms based on the detection-deletion scheme. *IEEE Transactions on Medical Imaging, 12*(2), 334–341.

Mallat, S., & Zhong, S. (1992). Characterization of signals from multiscale edges. *IEEE Transactions on Pattern Analysis and. Machine Intelligence, 4*, 710–732.

Martínez-Pérez, M. E., Hughes, A. D., Stanton, A. V., Thom, S. A., Bharath, A. A., & Parker, K. H. (1999). Retinal blood vessel segmentation by means of scale-space analysis and region growing. In *Proceedings of the 2nd MICCAI* (pp. 90–97).

Martínez-Pérez, M. E., Hughes, A. D., & Thom, S. A. (2007). Segmentation of blood vessels from red-free and fluorescein retinal images. *Medical Image Analysis, 11*, 47–61.

McInerney, T., & Terzopoulos, D. (2000). T-snakes: Topology adaptive snakes. *Medical Image Analysis, 4*, 73–91.

Mendonça, A. M., & Campilho, A. (2006). Segmentation of retinal blood vessels by combining the detection of centerlines morphological reconstruction. *IEEE Transactions on Medical Imaging, 25*(9), 1200–1213.

Nikam, S., & Agarwal, S. (2009). Ridgelet-based fake fingerprint detection. *Neurocomputing, 72*, 2491–2506.

Perfetti, R., Ricci, E., Casali, D., & Costantini, G. (2007). Cellular neural networks with virtual template expansion for retinal vessel segmentation. *IEEE Transactions on Circuits and Systems—II: Express Briefs, 54*, 141–145.

Pinz, S., Bernogger Datlinger, P., & Kruger, A. (1998). Mapping the human retina. *IEEE Transactions on Medical Imaging, 17*, 606–619.

Ricci, E., & Perfetti, R. (2007). Retinal blood vessel segmentation using line operators and support vector classification. *IEEE Transactions on Medical Imaging, 26*, 1357–1365.

Soares, J. V. B., Leandro, J. J. G., Cesar, R. M., Jr., Jelinek, H. F., & Cree, M. J. (2006). Retinal vessel segmentation using the 2-D Gabor wavelet and supervised classification. *IEEE Transactions on Medical Imaging, 25*(9), 1214–1222.

Sofka, M., & Stewart, C. V. (2006). Retinal vessel centerline extraction using multiscale matched filters, confidence and edge measures. *IEEE Transactions on Medical Imaging, 25*(12), 1531–1546.

Staal, J. J., Abràmoff, M. D., Niemeijer, M., Viergever, M. A., & van Ginneken, B. (2004). Ridge based vessel segmentation in color images of the retina. *IEEE Transactions on Medical Imaging, 23*(4), 501–509.

Steger, C. (1998). An unbiased detector of curvilinear structures. *IEEE Transactions on Pattern Analysis and Machine Intelligence, 20*, 113–125.

Sussman, E. J., Tsiaras, W. G., & Soper, K. A. (1982). Diagnosis of diabetic eye disease. *Journal of American Medical Association, 247*, 3231–3234.

Tamura, S., Okamoto, Y., & Yanashima, K. (1988). Zero-crossing interval correction in tracing eye-fundus blood vessels. *Pattern Recognition, 21*(3), 227–233.

Toledo, R., Orriols, X., Binefa, X., Radeva, P., Vitrià, J., & Villanueva, J. (2000). Tracking of elongated structures using statistical snakes. In *IEEE conference on CVPR* (Vol. 1, pp. 157–162).

Tolias, Y., & Panas, S. (1998). A fuzzy vessel tracking algorithm for retinal images based on fuzzy clustering. *IEEE Transactions on Medical Imaging, 17*, 263–273.

Vlachos, M., & Dermatas, E. (2010). Multi-scale retinal vessel segmentation using line tracking. *Computerized Medical Imaging and Graphics, 34*(3), 213–227.

Wilkinson, P., Ferris, F., Klein, R., Lee, P., Agardh, C., Davis, M., et al. (2003). Proposed international clinical diabetic retinopathy and diabetic macular edema disease severity scales. *Ophthalmology, 110*, 1677–1682.

Wu, D., Zhang, M., Liu, J. C., & Bauman, W. (2006). On the Adaptive Detection of Blood Vessels in Retinal Images. *IEEE Transactions on Biomedical Engineering, 53*(2), 341–343.

Zana, F., & Klein, J.-C. (2001). Segmentation of vessel-like patterns using mathematical morphology and curvature evaluation. *IEEE Transactions on Image Processing, 10*(7), 1010–1019.

Zhu, T. (2010). Fourier cross-sectional profile for vessel detection on retinal images. *Computerized Medical Imaging and Graphics, 34*(3), 203–212.